Simple synthesis of soft, tough, and cytocompatible biohybrid composites

Cameron Darkes-Burkey[a,1] , Xiao Liu[b,1], Leigh Slyker[c,1] , Jason Mulderrig[b], Wenyang Pan[b], Emmanuel P. Giannelis[a] , Robert F. Shepherd[b] , Lawrence J. Bonassar[b,c,2], and Nikolaos Bouklas[b,2]

Collagen is the most abundant component of mammalian extracellular matrices. As such, the development of materials that mimic the biological and mechanical properties of collagenous tissues is an enduring goal of the biomaterials community. Despite the development of molded and 3D printed collagen hydrogel platforms, their use as biomaterials and tissue engineering scaffolds is hindered by either low stiffness and toughness or processing complexity. Here, we demonstrate the development of stiff and tough biohybrid composites by combining collagen with a zwitterionic hydrogel through simple mixing. This combination led to the self-assembly of a nanostructured fibrillar network of collagen that was ionically linked to the surrounding zwitterionic hydrogel matrix, leading to a composite microstructure reminiscent of soft biological tissues. The addition of 5–15 mg mL^{-1} collagen and the formation of nanostructured fibrils increased the elastic modulus of the composite system by 40% compared to the base zwitterionic matrix. Most notably, the addition of collagen increased the fracture energy nearly 11-fold ($\Gamma = 180$ J m^{-2}) and clearly delayed crack initiation and propagation. These composites exhibit elastic modulus ($E = 0.180$ MJ) and toughness ($W^* = 0.617$ MJ m^{-3}) approaching that of biological tissues such as articular cartilage. Maintenance of the fibrillar structure of collagen also greatly enhanced cytocompatibility, improving cell adhesion more than 100-fold with >90% cell viability.

collagen network | hydrogel | composite | zwitterionic

The development of materials that match the mechanical performance of soft biological tissues while retaining high levels of biocompatibility has been an enduring challenge in the biomaterials community. Biological tissues achieve this high level of mechanical performance through the development of complex networks, often composed of collagen fibrils, that are ionically connected to a surrounding biological hydrogel. Hydrogels composed of extracellular matrix biopolymers such as collagen, fibrin, and hyaluronic acid have held significant interest due to their high cytocompatibility and in vivo degradability (1, 2). Of these, collagen hydrogels have been of particular interest due to their structural and compositional similarity to native extracellular matrices as they self-assemble to a fibrillar network. Notably, several collagen-based scaffolds are currently in advanced stage clinical trials for engineering tissues such as articular cartilage (e.g., MACI, NeoCart, NOVOCART 3D). Despite these advantages, however, collagen hydrogels have exhibited stiffness, toughness, and extensibility far below that of native tissues (3–5). For example, native cartilage has an elastic modulus between $E = 2$ and 10 MPa and toughness between $W^* = 0.01$ and 0.8 MJ m^{-3} (3, 5); collagen hydrogels, however, fall short with $E = 10$ to 14 kPa and $W^* = 2$ to 4 kJ m^{-3} (4).

Alternatively, a variety of synthetic materials have been developed with the goal of achieving the remarkable level of mechanical performance of soft biological tissues. Pioneering work (6) spurred widespread interest in double network hydrogel architectures that enable the combination of high toughness and extensibility (7–9) often found in biological tissues. Notably, this combination of stiffness and toughness is achieved through sacrificial rupture of covalent bonds that limits the resilience of these materials (10). More recently, several strategies were conceptualized to replace these sacrificial bonds with reformable ones (11, 12). One such approach involves the use of zwitterionic copolymer networks, in which ionic bonds enable energy dissipation through bond breakage and reformation (13–17). These materials have been explored for potential applications such as hydrogel implants (18–20) and passivation of biological surfaces (21–23). While this strategy leads to mechanical resilience, such materials have a limited ability to support cell adhesion and viability that are required for many applications in regenerative medicine.

Collectively, these data point to the need to develop a new strategy toward the design of stiff, tough, and cytocompatible materials. Here, we propose such a strategy

Significance

Soft tissues such as cartilage have limited capacity for regeneration. Synthetic materials that replicate both the mechanical and biological properties of soft tissues thus have the potential to replace damaged or degraded tissue. Synthetic polymer systems often lack both the ability to support and maintain live cells and the microstructural organization that supports their functionality. Conversely, natural polymers such as collagen, fibrin, and hyaluronic acid can replicate the biocompatibility of living tissues, but these materials are often soft and fragile. Here, we demonstrate the simple fabrication of a biohybrid hydrogel composite based on a zwitterionic hydrogel matrix and an interpenetrating self-assembled network of collagen fibers that leads to a biomimetic combination of stiffness, toughness, and cytocompatibility.

for the design of biohybrid collagen composites, in which the nanostructured collagen network interacts with a resilient synthetic hydrogel matrix. Specifically, we demonstrate that the introduction of a self-assembled nanostructured collagen network to a zwitterionic hydrogel matrix improves both stiffness and toughness while providing significant enhancement of cytocompatibility. These materials represent a major advance in mimicking the natural structure and properties of soft biological materials, and their simple synthesis has the potential to enable widespread use in regenerative medicine applications.

1. Results

1.1. Chemistry. To achieve the goal of a simple-to-formulate, stiff, tough, and cytocompatible composite, we mixed a zwitterionic hydrogel with an interconnected collagen network (Fig. 1A). The zwitterionic component was formed using acrylamide (AAM) and [2-(methacryloyloxy)ethyl] dimethyl-(3-sulfopropyl) ammonium hydroxide (DMAPS) as monomers that were cross-linked using poly(ethylene glycol) diacrylate (PEGDA), with riboflavin (RF) and triethanolamine (TEOHA) as the photoinitiator and coinitiator, respectively. Separately, collagen was prepared in a solution of acetic acid and phosphate-buffered saline (PBS) at pH 3.0 and stored at 4 °C. The zwitterionic and collagen solutions were mixed uniformly using syringes and a three-way stopcock. UV-initiation of the mixture led to the formation of the poly(AAM-co-DMAPS) copolymer network and the RF cross-linking collagen network, yielding composite materials at three different collagen concentrations ($\varphi_{collagen} = 5$, 10, and 15 mg mL^{-1}) at pH 7.0.

We describe this material as a composite due to the self-assembly of collagen into a nanostructured fibrillar network that is ionically connected to the zwitterionic matrix. The microstructure of the composite contained a hierarchy of features in the two phases (Fig. 1B). Notably, ionic bridges form between the charges
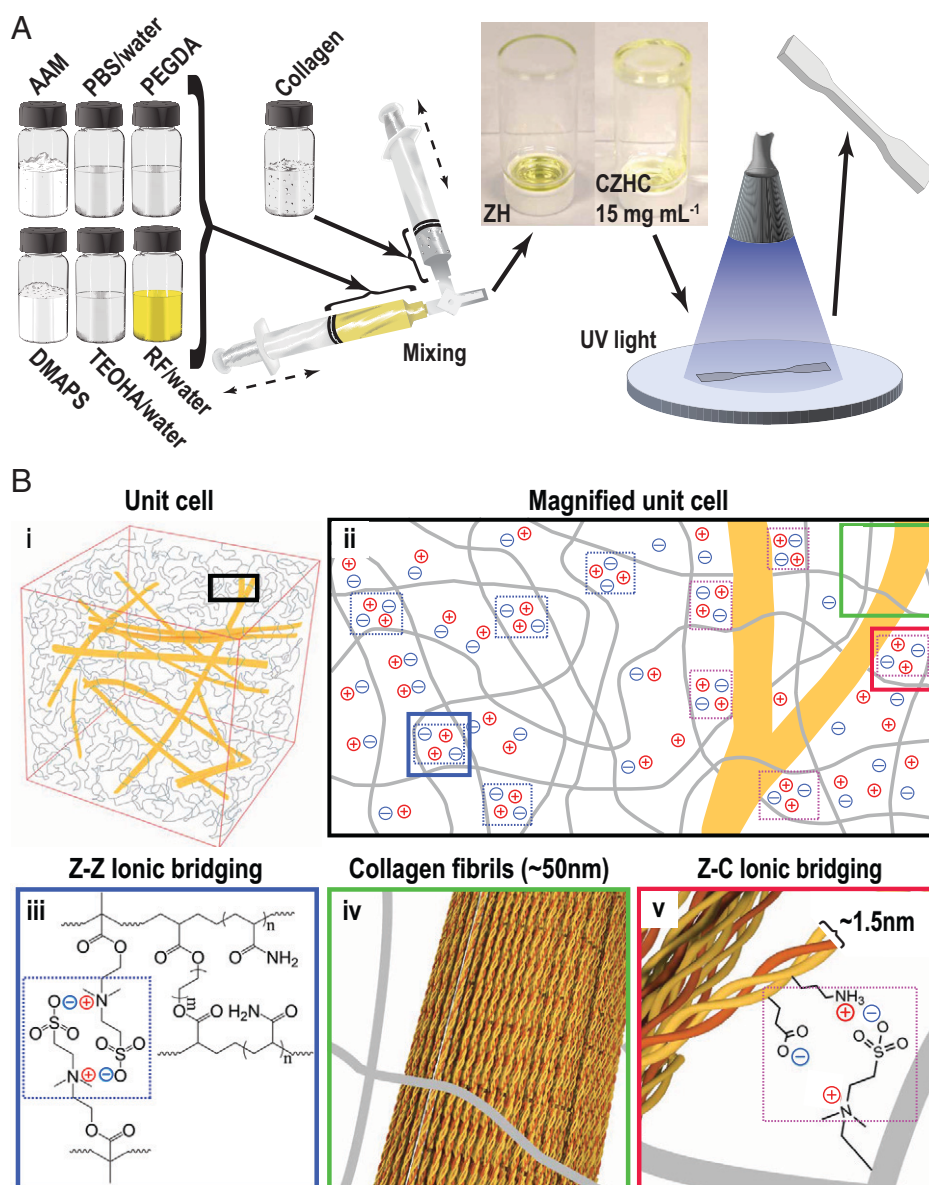
Fig. 1. Chemistry schematic. (A) Two-step fabrication process of composite with a visual comparison of viscosity differences between the zwitterionic gel and the composite. (B) Schematic illustration of the composite system, combining zwitterionic matrix and a collagen fibrillar network (*i* and *ii*). The zwitterionic matrix, based on AAM and DMAPS, carries ionic bridging between the zwitterionic charged groups and is covalently cross-linked by *N-N'* methylenebisacrylamide (*iii*). The fibrillar network is composed of self-assembled collagen fibrils (*iv*) and the final composite is enabled through ionic bridging between the zwitterionic matrix and the collagen fibrillar network (*v*). Orange and yellow collagen helix strands represent α2 and α1 chains, respectively.

on the zwitterionic moieties (anionic sulfonate groups and cationic quaternary amine groups) and the collagen (anionic carboxylic acid groups, primarily aspartate and glutamate, and cationic groups, primarily lysine; Fig. 1*B, ii, iii, v*). These ionic interactions have been shown to play an important role in mechanically stabilizing and strengthening the network (13, 15, 19, 20). The microstructure of the interpenetrating network of collagen fibrils can play an important role in toughening the composite gel, as has been seen in other hydrogel composites with nanostructured components (Fig. 1*B, iv*) (24, 25).

1.2. Scanning Electron Microscopy (SEM). The enhancement of the mechanical performance of the base zwitterionic hydrogel would be enabled by the formation of an interpenetrating fibrillar network. The presence of self-aggregated collagen fibrils within the bulk of the zwitterionic gel was clearly demonstrated using SEM. At low magnification, these fibrils are evident in $\varphi_{collagen} = 10$ mg mL^{-1} and $\varphi_{collagen} = 15$ mg mL^{-1} samples (Fig. 2*G* and *J*), as compared to the smooth surfaces of $\varphi_{collagen} = 5$ mg mL^{-1} and the control, $\varphi_{collagen} = 0$ mg mL^{-1} gels (Fig. 2*A* and *D*). The presence of distinct collagen fibrils becomes clear in 10 and 3 μm field of view images of $\varphi_{collagen} = 5, 10,$ and 15 mg mL^{-1} gels (Fig. 2*E, F, H, I, K,* and *L*). For low collagen concentrations, fibrils appear to be smaller and more isolated (Fig. 2*E* and *F*), whereas high collagen concentration gels have long, thick, and well-connected fibrillar domains (Fig. 2*H, I, K,* and *L*). These observations confirm that a collagen fibrillar network self-aggregates with interpenetrating topology within the zwitterionic gel matrix. With increasing collagen concentration, the collagen fibrillar network also better resembles that of collagen-only gels (Fig. 2*M–O*). Absorbance at 600 nm of samples pre- and postgelation provided additional confirmation of the self-aggregation and fibrillogenesis (*SI Appendix,* Fig. S5*A–C*). Interestingly, this self-aggregation resulted from the simple two-step fabrication process depicted in Fig. 1, contrasting with more complicated synthesis procedures of comparable recently developed bioinspired composites (26, 27).

1.3. Mechanical Testing. An enduring challenge of biomaterials design is to make cytocompatible materials for tissue regeneration and replacement that are as stiff and tough as their native counterparts. We use two separate protocols to assess the mechanical properties of the composite. Two types of tensile test samples were prepared: pristine dog bone samples were used for measuring elastic modulus and toughness (often referred to as work to rupture), whereas rectangular samples with a sharp crack were used for a single edge notch test to measure the fracture energy. To evaluate these parameters, we prepared samples for pure collagen hydrogel, pure zwitterionic hydrogel, and composites at $\varphi_{collagen} = 5, 10,$ and 15 mg mL^{-1}.

For all zwitterionic and composite gel curves, uniaxial testing for pristine dog bone samples showed a short initial section of slightly higher stiffness followed by a slight and gradual decrease until the sample fails. The response remained relatively linear through the range of loading. For the zwitterionic gel samples, the decrease in stiffness occurred earlier, followed by a linear regime until failure. Select representative curves from these tests are shown alongside results from a pure collagen gel. Notably, the composite showed an increase in modulus as well as an increase in toughness compared to both the zwitterionic hydrogel and collagen hydrogel (Fig. 3*A*). Here, toughness is the total area under the curve representing the work to rupture in the absence of macroscopic defects such as cracks.

The elastic modulus from these samples was $E = 2.81, 293,$ and 361 kPa for the collagen hydrogel, zwitterionic hydrogel, and composite samples, respectively. This stiffening was dependent on the amount of collagen in the composite. For collagen content of $\varphi_{collagen} = 5, 10,$ and 15 mg mL^{-1}, the composite gel had an elastic modulus $E = 359.6 \pm 17.8$ kPa, 375.2 ± 9.3 kPa, and 377.1 ± 35.1 kPa, respectively ($P < 0.002$ vs. milligrams per milliliter of collagen).

The combination of stiffness and toughness is critical for the resilience of a material. Thus, we compared the elastic modulus and toughness of our composite material to other hydrogel systems from the literature (Fig. 3*C*), namely, collagen hydrogels (4) and collagen hydrogel composites (4, 28–30), as well as the control zwitterionic hydrogel and native articular cartilage (31) as a benchmark. The combination of stiffness and toughness observed in the collagen zwitterionic composites in this study exceeds those of previously reported collagen-based systems. Furthermore, our system approaches the properties of native articular cartilage in tension, achieving similar toughness with approximately an order of magnitude lower modulus.

A potential advantage of ionically coupled materials is their resilience under repeated loading, due to the breaking and reformation of ionic bonds, as they allow for energy dissipation without inducing permanent damage. To assess this resilience, cyclic testing was performed under displacement control. These experiments showed good repeatability of this composite under multiple loading cycles (*SI Appendix,* Fig. S1). Specifically, the specimen exhibited minimal modulus loss between cycles despite being loaded up to 90% of the ultimate failure strain. This resilience contrasts with covalently linked systems, such as double network hydrogels, in which a significant modulus loss is observed after a single loading cycle (32).

Toughness experiments are sensitive to preexisting microscopic defects and their corresponding distributions (4, 28, 30). Therefore, variability in synthesis and manufacturing conditions make it difficult to compare the true energy expended in rupturing between samples. To measure the fracture energy Γ (33–35) as a function of collagen content, we therefore prescribed where rupture would initiate by applying a sharp crack one-third of the width of the sample to each sample before loading. Testing samples this way allows precise control of the size of the largest defect, as the induced crack can be designed to be several orders of magnitude larger than the preexisting defects, thus dominating the response.

The presence of collagen had a dramatic influence on the fracture energy of the composite samples. Snapshots of the samples during testing showed significant blunting of the crack tip for a collagen content of $\varphi_{collagen} = 15$ mg mL^{-1} (Fig. 3*D*) before and during crack propagation. The stress-strain curve is close to linear up until the crack point and shows a gradual decrease in engineering stress as the crack continues to propagate. Video tracking showed that the 2.5-mm crack first started to propagate at an overall engineering strain of $\varepsilon_{crit}^{eng} = 0.25$ and a critical far-field engineering stress of $\sigma_{crit}^{eng} = 0.116$ MPa, noting that these values depend on the initial crack length. Fracture energy increased monotonically with collagen concentration in the composite ($P < 10^{-8}$, ANOVA on toughness and collagen concentration; Fig. 3*E*). The presence of 15 mg mL^{-1} collagen in the composite gel increased the fracture energy 11-fold, with the zwitterionic gel $\Gamma = 16.85 \pm 2.60$ J m^{-2} and the $\varphi_{collagen} = 15$ mg mL^{-1} composite $\Gamma = 180.21 \pm 8.82$ J m^{-2}.

1.4. Cell Seeding. To document the effect of the addition of collagen on cytocompatibility, we seeded bovine articular chondrocytes
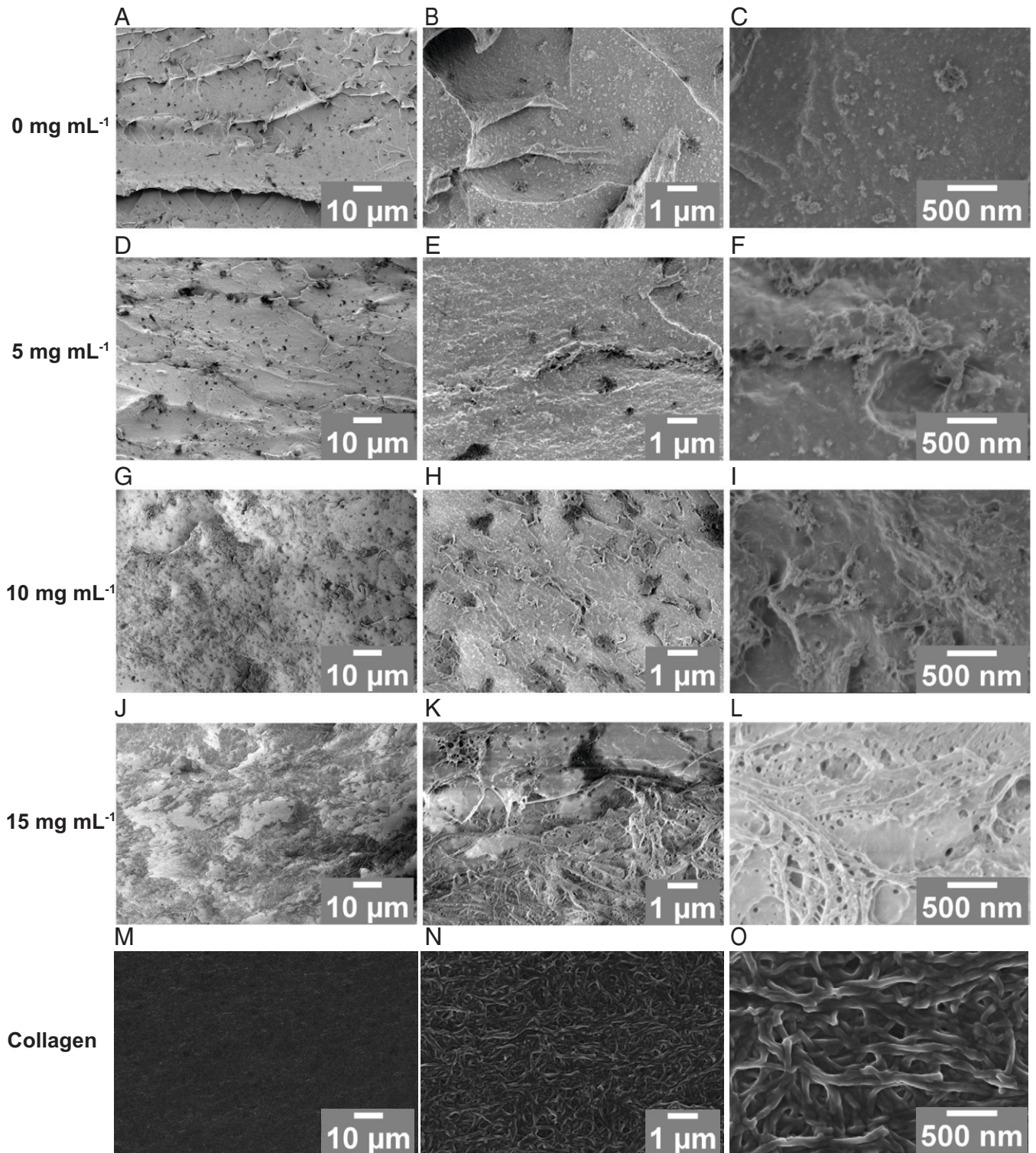
Fig. 2. SEM of gels. SEM of collagen-zwitterionic gels with $\varphi_{collagen} = 0$ (*A–C*), 5 (*D–F*), 10 (*G–I*), and 15 (*J–L*) mg mL^{-1} collagen, and 8 mg/mL collagen gels (*M–O*) as labeled, with increasing magnification from left to right.

on the surface of composite and zwitterionic gels and measured cell viability and attachment. Staining of composite gels seeded with chondrocytes revealed a high overall viability with an increase in overall cell count with increasing collagen concentration evident from confocal images (Fig. 4 *A–C* and SI Appendix, Fig. S4). The quantification of cell viability revealed increased viability in composite gels at $\varphi_{collagen} = 5$ ($P < 10^{-4}$), 10 ($P < 10^{-4}$), and $\varphi_{collagen} = 15$ mg mL^{-1} ($P < 10^{-4}$) collagen, as compared to

zwitterionic gels (Fig. 4*D*). The number of live cells increased with increasing collagen concentration, with fewer live cells on $\varphi_{collagen} = 0$ mg mL^{-1} than $\varphi_{collagen} = 5$ mg mL^{-1} ($P = 0.046$), 10 mg mL^{-1} ($P < 10^{-3}$), and 15 mg mL^{-1} ($P < 10^{-3}$) gels (Fig. 4*E*). The number of dead cells did not differ between collagen concentrations (Fig. 4*F*).

SEM of cell-seeded gels provided further evidence of differential cell attachment between composite and zwitterionic
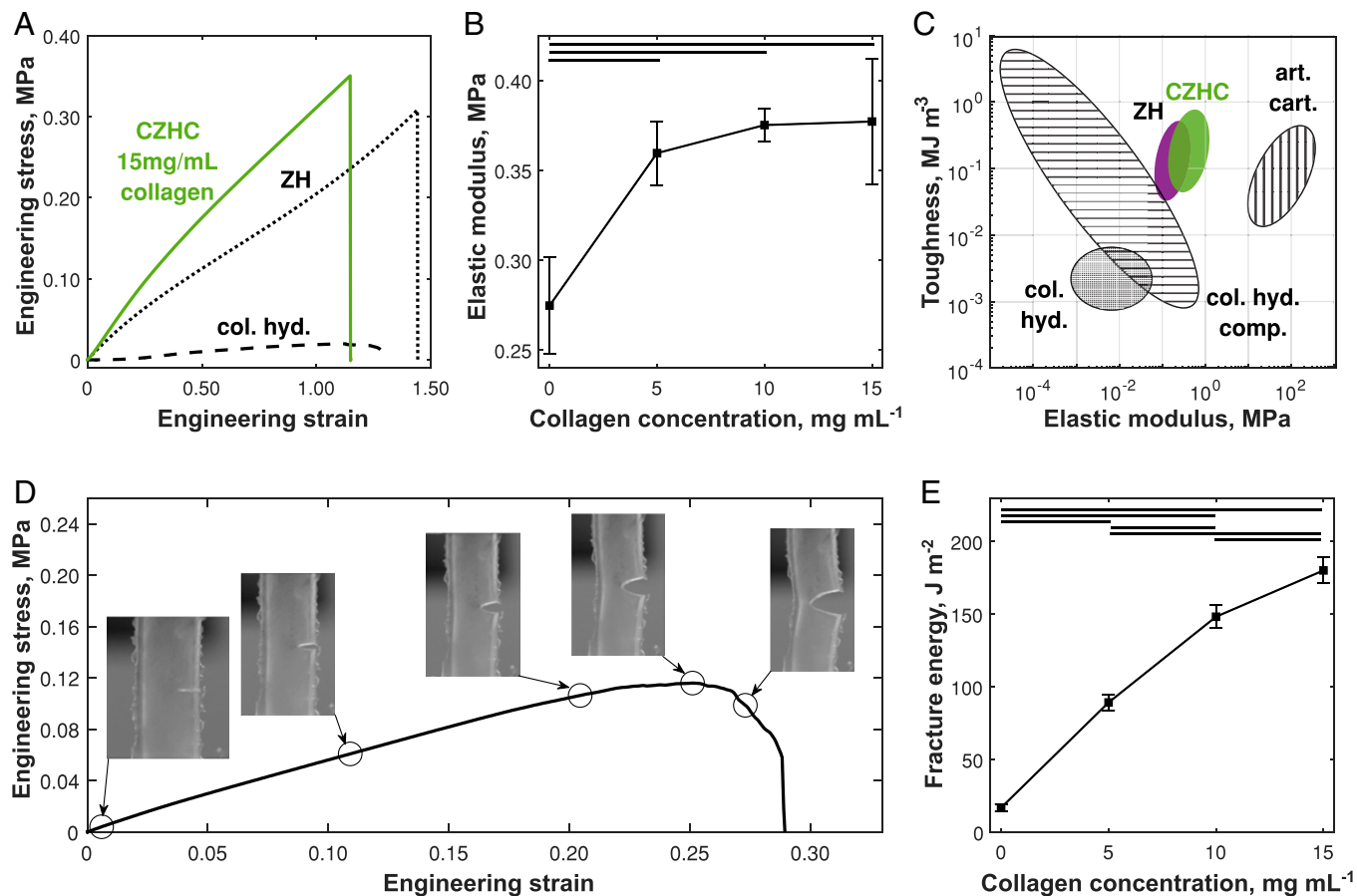
Fig. 3. Mechanical properties. (*A*) Comparison of molded stress-strain curves of our collagen-zwitterionic hydrogel composite against its components. (*B*) Elastic modulus of our collagen composite system with different collagen loadings. (*C*) Mechanical property comparison of our collagen-zwitterionic hydrogel composite with other tough hydrogel systems and articular cartilage. Representative stress vs. strain curve (*D*) of the notch test at $\varphi_{collagen}$ = 15 mg mL^{-1} collagen as well as fracture energy results (*E*) at various collagen loadings. All of the error bars represent 1 SD above and below the mean. All of the tests were run in triplicate. All of the horizontal bars represent statistical significance between groups ($P < 0.05$).

hydrogels. No cells were found on zwitterionic gels through SEM, likely due to the low number of live cells present after culture (Fig. 4*E*). However, the presence of cells was evident on all composite gels, with the majority of cells found on collagen-rich domains of the gel surface (Fig. 4*G*). Cells directly attached to large fibril aggregates appeared to have better attachment (Fig. 4*G* and *H*), whereas cells on synthetic domains appear rounded and poorly attached (Fig. 4*G*). Some cells attached to collagen-rich domains also facilitated matrix deposition as evidenced by fibrils overlying and securing the cell to the composite gel (Fig. 4*H*).

2. Discussion

The goal to mimic and recreate biological tissues with synthetic materials is one that has challenged the biomaterials community for decades. In this study, we synthesized a material that mimics the structure of many biological tissues: a fibrillar collagen network reinforced by an ionically active gel. This collagen-zwitterionic gel composite exhibited a combination of stiffness and toughness that approached native connective tissues and had high cytocompatibility for cells seeded on its surface.

The benefits of adding an interpenetrating collagen network to a zwitterionic hydrogel were remarkable. Even at an exceedingly low weight fraction ($\varphi_{collagen} \ll 0.015$), the addition of collagen increased elastic modulus by 40% ($E = 377.1 \pm 35.1$ kPa vs. $E = 274.7 \pm 26.8$ kPa), and fracture energy by almost 11-fold ($\Gamma = 16.85 \pm 2.60$ J m^{-2} vs. $\Gamma = 180.21 \pm 8.82$ J m^{-2}). These values represent an increase of two orders of magnitude in toughness and an order of magnitude increase in stiffness over previously reported collagen hydrogel composites (4, 28–30). Furthermore, the addition of collagen greatly enhanced cell viability (~90%) and attachment, likely due to the role of integrins in facilitating the attachment of chondrocytes to type I collagen (36, 37). Although the use of fetal bovine serum (FBS) in culture may have facilitated the attachment of chondrocytes to the collagen matrix, it is clear that zwitterionic gels alone do not facilitate the association of the proteins in FBS. Thus, while the specific proteins that facilitate attachment of chondrocytes to the matrix were not investigated, the enhancement of cell attachment due to the addition of collagen is dramatic.

Collagen-zwitterionic composites contained nanostructured collagen fibrils that formed an interconnected network, as confirmed by SEM. The fibrous collagen network increased the modulus and toughness of material, but it also facilitated cellular attachment and remodeling. As such, this composite has the potential for use in engineering of soft tissues such as articular cartilage. In addition, since the zwitterionic hydrogel can be 3D printed, the system could be used in engineering tissues with arbitrary geometries through digital light processing (16).

A key driver of the mechanical contributions of the self-assembled composite architecture is network connectivity. To estimate the network connectivity as a function of collagen content of the composite based on experimental measurements of elastic
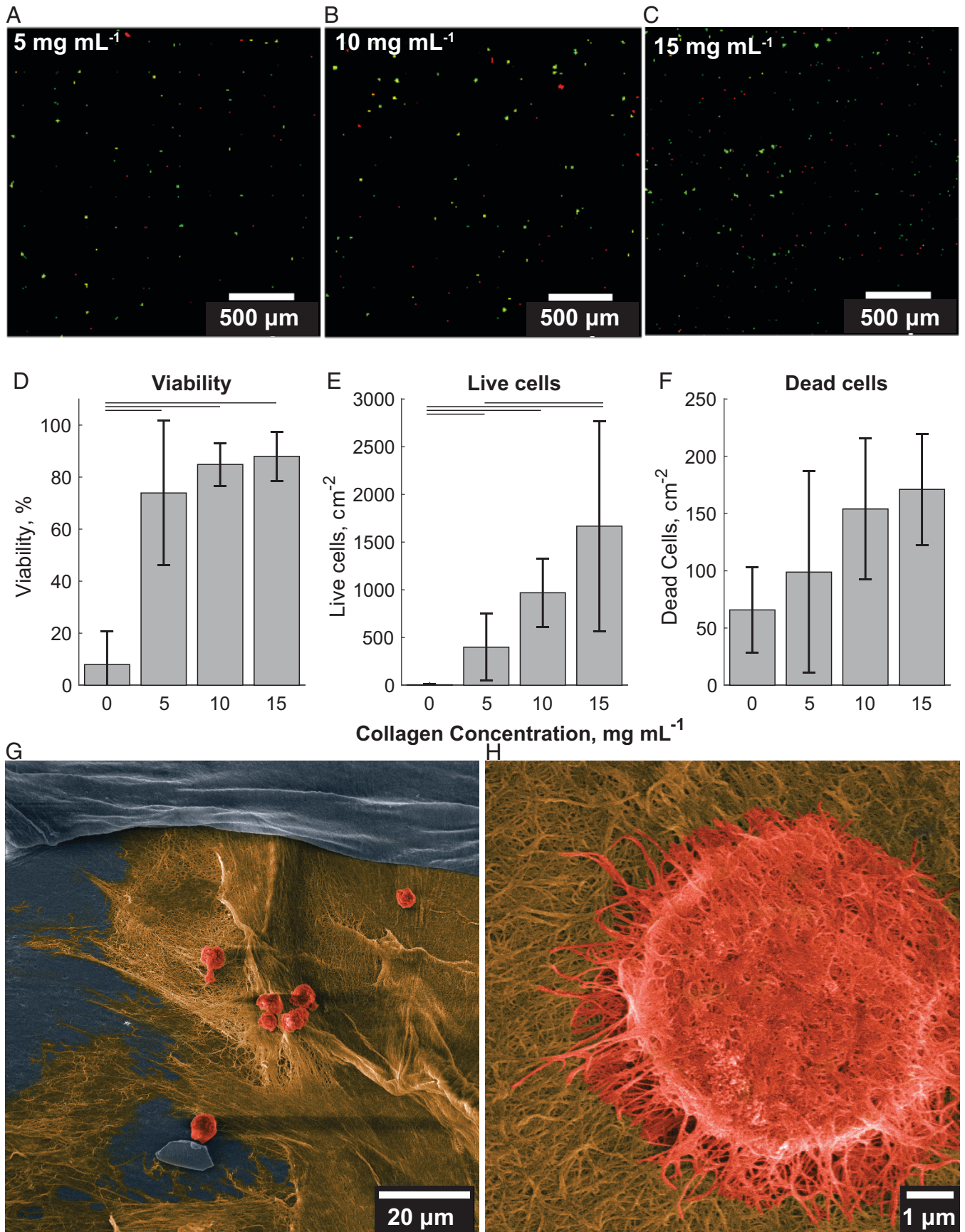
Fig. 4. Cell viability results. (*A–C*) Live-dead staining of composite gels with collagen concentrations of $\varphi_{collagen}$ = 5, 10, and 15 mg mL^{-1}. (*D*) Percent viability of seeded cells. Bars indicate significant differences between groups ($P < 0.05$). (*E*) Live cells per square centimeter of gel surface. (*F*) Dead cells per square centimeter of gel surface. (*G*) Colored SEM micrographs of cells (red) seeded on the fibrous domain (yellow) of $\varphi_{collagen}$ = 5 mg mL^{-1} gel. (*H*) SEM micrograph of cell (red) seeded on $\varphi_{collagen}$ = 10 mg mL^{-1} gel with evidence of fibril deposition by cell. Error bars represent 1 SD above and below the mean. Horizontal bars represent statistical significance between groups ($P < 0.05$).

modulus and fibril geometry, we used an analysis outlined in *SI Appendix,* Section S1. In summary, we used the rule of mixtures, SEM data for collagen fibril geometry, and existing scaling laws for collagen network elasticity. The results showed that the collagen fibrils are, on average, connected in branched junctions (average network connectivity ≈3), leading to an interconnected network topology. This level of network connectivity further confirms the efficacy of the two-step fabrication process depicted in Fig. 1*A* to create a fully percolated and mechanically functional collagen fibril network interpenetrated within the zwitterionic gel matrix (38).

A major feature of the fabrication process of this material is that the self-assembly of the collagen fibrils network within the zwitterionic hydrogel is achieved by simple mixing. Other methods to achieve similar composite architectures are significantly more complex. For example, electrospun (39–42) and UV-cured double network hydrogels (26, 43, 44) often require multiple time-intensive synthetic stages. Recent advances in electrochemically aligned threads have yielded large diameter fibrils with significantly improved tensile modulus and strength; however, this process requires many hours to days of synthesis (45). These large-scale fibers have the potential to further increase modulus and strength in our composite material. In addition, large-scale fibers would better match those present in connective tissues, which have diameters in the range of 1–50 μm (46).

With these advantages in mind, this research demonstrates the creation of a self-assembled collagen zwitterionic hydrogel composite with potential in tissue engineering. This advance enables a wide range of applications, in which a combination of strong mechanical properties, great cytocompatibility, and good native tissue integration is required simultaneously, including regenerative tissue engineering such as synthetic cartilage.

3. Experimental Design

3.1. Materials. AAM (≥99%), DMAPS (95%), PEGDA (M_w 575), (PBS) tablets, and acetic acid were purchased from Sigma-Aldrich (St. Louis, MO). RF and TEOHA were obtained from Neta Scientific (Hainesport, NJ). Antibiotic-antimycotic solution and Dulbecco's modified Eagle's medium (DMEM) were obtained from Corning (Manassas, VA). Chemicals were used as received without further purification. Millipore Milli-Q water (resistivity >18 $M\Omega \ cm^{-1}$ at 25 °C) and deionized (DI) water were used in the experiments.

Collagen was prepared through extraction from rat tail tendons, as previously described (47). Briefly, rat tail tendons were solubilized in 0.1% acetic acid at a concentration of 6.67 g L^{-1} at 4 °C for a minimum of 48 h. Solutions were centrifuged at 9,000 rpm for 90 min at 4 °C, with lyophilization of the supernatant to yield a collagen sponge. The lyophilized collagen was then reconstituted in 0.1% acetic acid at a concentration of 30 mg mL^{-1} and stored at 4 °C.

3.2. Resin Preparation. The zwitterionic hydrogel resin was prepared as described previously (16), except that the N,N'-methylenebisacrylamide cross-linker was replaced by PEGDA for lower cytotoxicity (48, 49). Briefly, 2.8 M AAM, 0.7 M DMAPS, and 1 mol% of PEGDA were dissolved in 10X PBS buffer and Milli-Q water to a final PBS concentration of 1×. To the mixture 10^{-5} M, RF was added as the photoinitiator and the pH was adjusted to ~7.0 using TEOHA (30% wt/vol as stock solution). TEOHA also serves as the coinitiator of the reaction.

The collagen zwitterionic hydrogel composite resin was prepared by mixing certain amounts of collagen (30 mg/mL in 0.1% acetic acid stock solution) with a concentrated zwitterionic hydrogel resin using a polycarbonate three-way stopcock (50) (Cole-Parmer, Vernon Hills, IL). All final solutions had a PBS concentration of 1×. All of the resins were stored at 4 °C. The final pH of the collagen zwitterionic hydrogel composite resins was adjusted by adding TEOHA dropwise before use. All of the samples were prepared at pH 7.0.

3.3. Sample Preparation. Tensile test samples were prepared using a transparent Sylgard184 mold. ISO 527–2 Type 5A samples with a gauge length of 25 mm and a thickness of 2 mm were prepared as the pristine dog bone samples. Single-edge notch test samples were prepared from rectangular samples 7.5 × 50 × 1.5 mm. A 2.5-mm crack was cut into the edge of the sample with a razor blade jig at approximately the halfway point along the long edge of the sample. Photocurable resin was added to the mold and an Omnicure S1500 UV light source (Excelitas Technologies, Waltham, MA) was used to form the tensile test samples. Curing time was selected as 20 min, with the light source being held 10 cm away from the surface of the sample to ensure that the samples were fully cured. The specifications of the light source can be found in *SI Appendix,* Fig. S3.

3.4. SEM. Following incubation for 2 h at 37 °C, collagen gels were sectioned using a 4-mm biopsy punch. Sections were cross-linked with 4% formalin in PBS for 1 h before rinsing 3 times with PBS and twice with DI water for 10 min each. Gel sections were then cross-linked with 1% osmium tetroxide for 1 h and dehydrated with a graded series of ethanol/water washes (30%, 50%, 70%, 90%, then 100% [×2] ethanol in water), followed by a graded series of hexamethyldisilazane/ethanol washes (33%, 50%, 66%, 100% hexamethyldisilazane in ethanol). Gels were dried overnight at room temperature and pressure, followed by vacuum drying for 48 h (51). After drying, gels were grounded to sample pins with silver conductive paint and gold foil and sputter coated with an Au/Pd alloy for 20 s at a target current of 20 mA. Sputter-coated samples were then imaged with a field of view of 3, 10, and 100 μm at an accelerating voltage of 0.5 to 2 kV and a working distance of 5 mm.

3.5. Mechanical Testing. Tensile tests were performed using the Zwick & Roell Z1010 testing machine (Ulm, Germany) at a strain rate of 10 mm/min (52).

Due to the flexible and tacky nature of many of the samples, care was taken to properly clamp the samples in the tensile grips using sandpaper to provide extra friction.

Tests were run with samples containing 4 different collagen loadings ($\varphi_{collagen}$ = 0, 5, 10, and 15 mg mL^{-1}), with the $\varphi_{collagen}$ = 0 mg mL^{-1} loading being just the zwitterionic hydrogel control. Tests were run in triplicate for reproducibility. Elastic modulus values were calculated as the initial slope of the stress-strain curves of the pristine samples up until an initial engineering strain of γ^{eng} = 0.05. Single-edge notch test samples were used to calculate fracture energy values according to methods described by Chen et al. and Tutwiler et al. (34, 35) (see below).

Representative cyclic tensile tests were performed to test the samples after many loading cycles. Speeds of 10 mm min^{-1} up to 75% of the failure strain determined from previous strain-to-failure measurements were used for $\varphi_{collagen}$ = 10 mg mL^{-1} gels. Cyclic tensile tests with a rest period at full extension of the samples were also performed. The samples were held at constant strain for triple the time it took for the sample to reach full extension.

3.6. Fracture Energy Calculation. The fracture energy of the samples was calculated using the method by Chen et al. (34). The energy release rate, $G(\lambda, c)$, or the reduction in elastic energy when the cut extends per unit area, is defined as $G(\lambda, c) = -\delta U(\Delta, c)/t\delta c$, where $U(\Delta, c)$ is the elastic energy of the system at displacement Δ, c is crack length, t is the thickness of the sample, and λ is the stretch of the sample. When all of the other dimensions are much larger than the crack length, the energy release rate can be set equal to $G(\lambda, c) = k(\lambda) W(\lambda) c$, where $k(\lambda)$ is the stress intensity factor for the given stretch and $W(\lambda)$ is the strain energy density, or the area under the force-displacement curve divided by the volume of the unstretched material for the pristine dog bone sample as a function of stretch. The stress intensity factor is a dimensionless parameter determined by solving the boundary-value problem. When other dimensions of the sample are much larger than the cut, the only dimension in the boundary value problem is the length, c. As the sample is stretched, the sample will eventually rupture at a stretch of λ_R, when the critical energy release rate is equal to the fracture energy, $G_c(\lambda_R, c) = \Gamma$, where Γ is the fracture energy of the material. Substituting the fracture energy for the energy release rate and rearranging, we obtain an expression for the fracture energy: $\Gamma = k(\lambda_R) W(\lambda_R) c$. When the length of the cut is large (one-third of the width of the sample) and the sample ruptures at a small strain, we can apply linear elasticity with $\lambda \to 1$. For small deformations, the stress intensity factor is $k(1) \approx 2(1.1215)^2\pi \approx 7.90$ (53). As the stress-strain curves of our samples are essentially linear up until crack propagation, we can consider that the above holds for the majority of the specimens as they fail in moderately small deformations.

To confirm the reliability of this approach, a second method was also used for the samples at 15 mg mL^{-1}, which had the largest failure strains. In this approach, we do not use the stress-intensity factor to eventually arrive at the fracture energy. We start by rewriting the equation for the reduction in elastic energy under the condition that the crack has just started propagating and the crack is still at its initial length $c = c^*$.

$$G_c(\lambda_R, c) = -\frac{\delta U(\Delta_R, c)}{t\delta c} \mid c = c^*, \qquad [1]$$

where λ_R and Δ_R are the critical stretch and displacement, respectively, when the crack starts to propagate. For our experiments, similar to Tutwiler et al. (35), the force-displacement curves were nearly linear up until the crack propagated, so $U(\Delta_c^*, c) \approx \frac{1}{2}\Delta_c^{*2}\left(\frac{F}{\Delta}\right)$, where F is the applied force. Substituting this into Eq. **1** gives

$$\Gamma \approx -\frac{1}{2t}\Delta_c^{*2}\left(\frac{d\left(\frac{F}{\Delta}\right)}{dc}\right) \mid c = c^*. \qquad [2]$$

Using a camera to record the uniaxial tension tests of the single-edge notch test samples, we were able to match up the raw force and displacement data with the length of the crack at each time point. This allowed us to approximate the derivative of the F/Δ vs. c curve at the point where the crack starts to propagate. We compared the results of these two methods for the 15 mg mL^{-1} samples under varied pH conditions (*SI Appendix*, Fig. S2). For pH 6.5, 7.0, and 7.5 ($\lambda_c^* = 1.261$, 1.268, and 1.242, respectively), the methods differ by less than 25%. The pH 8.0 results differ by 77%, whereas at pH 8.5, the results differ by almost 600%. The results at pH 7.0 for both models (the nonlinear elastic model result is displayed in Fig. 3) are not statistically different, confirming the reliability of either method. We conclude that for pH 8.0 ($\lambda_c^* = 1.271$), the small strain assumption starts to diverge, and at pH 8.5 ($\lambda_c^* = 1.371$), it no longer holds true.

3.7. Cell Surface Seeding. The hydrogels were first rinsed with ethanol and PBS 6 times for a minimum of 10 min each to ensure sterility. Chondrocytes were isolated from articular cartilage from bovine stifle joints as described previously. Gels were then placed in individual wells in a 24-well plate and seeded with primary bovine articular chondrocytes at a density of 5,000 cells per square centimeter (50, 54). Seeded hydrogels were then incubated in DMEM with 10% FBS and antibiotic-antimycotic (1X) at 37 °C for 4 d. Afterward, the culture gels were rinsed with PBS and stained with calcein AM and ethidium homodimer-1 for 20 min. After rinsing with PBS, the gels were covered with PBS to prevent drying and immediately imaged on an inverted confocal microscope with a 10X/0.45 water immersion objective. Live/dead imaging was achieved with an excitation wavelength of 488 nm and emission filters for live and dead cells set at 510 to 560 nm and 610 to 660 nm, respectively. Live and dead cells were counted with a custom MATLAB code (55).

3.8. Statistics. All of the measurements were performed in triplicate unless otherwise stated. Statistical analysis was performed using RStudio (version 1.2.1335 for Windows). The effects of collagen concentration on the mechanics and cell-seeding results were compared using a one-way ANOVA with Tukey honestly significant difference post hoc test, with significance set at $P = 0.05$. Data are presented as means $\pm$ SDs.

Author affiliations: [a]Department of Materials Science and Engineering, Cornell University, Ithaca, NY 14850; [b]Sibley School of Mechanical and Aerospace Engineering, Cornell University, Ithaca, NY 14853; and [c]Nancy E. and Peter C. Meinig School of Biomedical Engineering, Cornell University, Ithaca, NY 14853

1. A. J. Sophia Fox, A. Bedi, S. A. Rodeo, The basic science of articular cartilage: Structure, composition, and function. *Sports Health* **1**, 461–468 (2009).
2. M. Liu *et al.*, Injectable hydrogels for cartilage and bone tissue engineering. *Bone Res.* **5**, 1–20 (2017).
3. A. R. Armiento, M. J. Stoddart, M. Alini, D. Eglin, Biomaterials for articular cartilage tissue engineering: Learning from biology. *Acta Biomater.* **65**, 1–20 (2018).
4. T. R. Anderson, M. E. Marquart, A. V. Janorkar, Effective release of a broad spectrum antibiotic from elastin-like polypeptide-collagen composite. *J. Biomed. Mater. Res. A* **103**, 782–790 (2015).
5. K. Stok, A. Oloyede, Conceptual fracture parameters for articular cartilage. *Clin. Biomech. (Bristol, Avon)* **22**, 725–735 (2007).
6. J. P. Gong, Y. Katsuyama, T. Kurokawa, Y. Osada, Double-network hydrogels with extremely high mechanical strength. *Adv. Mater.* **15**, 1155–1158 (2003).
7. J. P. Gong, Why are double network hydrogels so tough? *Soft Matter* **6**, 2583 (2010).

8. L. Weng, A. Gouldstone, Y. Wu, W. Chen, Mechanically strong double network photocrosslinked hydrogels from N,N-dimethylacrylamide and glycidyl methacrylated hyaluronan. *Biomaterials* **29**, 2153–2163 (2008).
9. K. Yasuda *et al.*, Biomechanical properties of high-toughness double network hydrogels. *Biomaterials* **26**, 4468–4475 (2005).
10. Y. C. Fung, *Biomechanics: Mechanical Properties of Living Tissues* (Springer, New York, 1993)).
11. J.-Y. Sun *et al.*, Highly stretchable and tough hydrogels. *Nature* **489**, 133–136 (2012).
12. J. Odent *et al.*, Highly elastic, transparent, and conductive 3D-printed ionic composite hydrogels. *Adv. Funct. Mater.* **27**, 1701807 (2017).
13. K. J. Henderson, T. C. Zhou, K. J. Otim, K. R. Shull, Ionically cross-linked triblock copolymer hydrogels with high strength. *Macromolecules* **43**, 6193–6201 (2010).
14. X. Zhao, J. Liang, G. Shan, P. Pan, High strength of hybrid double-network hydrogels imparted by inter-network ionic bonds. *J. Mater. Chem. B Mater. Biol. Med.* **7**, 324–333 (2019).

15. C. W. Peak, J. J. Wilker, G. Schmidt, A review on tough and sticky hydrogels. *Colloid Polym. Sci.* **291**, 2031–2047 (2013).
16. W. Pan et al., Optical stereolithography of antifouling zwitterionic hydrogels. *J. Mater. Chem. B Mater. Biol. Med.* **7**, 2855–2864 (2019).
17. W. Diao et al., Highly stretchable, ionic conductive and self-recoverable zwitterionic polyelectrolyte-based hydrogels by introducing multiple supramolecular sacrificial bonds in double network. *J. Appl. Polym. Sci.* **136**, 47783 (2019).
18. L. Zhang et al., Zwitterionic hydrogels implanted in mice resist the foreign-body reaction. *Nat. Biotechnol.* **31**, 553–556 (2013).
19. L. R. Carr, Y. Zhou, J. E. Krause, H. Xue, S. Jiang, Uniform zwitterionic polymer hydrogels with a nonfouling and functionalizable crosslinker using photopolymerization. *Biomaterials* **32**, 6893–6899 (2011).
20. L. R. Carr, J. E. Krause, J.-R. Ella-Menye, S. Jiang, Single nonfouling hydrogels with mechanical and chemical functionality gradients. *Biomaterials* **32**, 8456–8461 (2011).
21. Y. Jiang, B. Rongbing, T. Ling, S. Jian, L. Sicong, Blood compatibility of polyurethane surface grafted copolymerization with sulfobetaine monomer. *Colloids Surf. B Biointerfaces* **36**, 27–33 (2004).
22. S. L. West et al., The biocompatibility of crosslinkable copolymer coatings containing sulfobetaines and phosphobetaines. *Biomaterials* **25**, 1195–1204 (2004).
23. W. Yang et al., The effect of lightly crosslinked poly(carboxybetaine) hydrogel coating on the performance of sensors in whole blood. *Biomaterials* **33**, 7945–7951 (2012).
24. S. Lin et al., Anti-fatigue-fracture hydrogels. *Sci. Adv.* **5**, eaau8528 (2019).
25. S. Lin, J. Liu, X. Liu, X. Zhao, Muscle-like fatigue-resistant hydrogels by mechanical training. *Proc. Natl. Acad. Sci. U.S.A.* **116**, 10244–10249 (2019).
26. F. Yang et al., A synthetic hydrogel composite with the mechanical behavior and durability of cartilage. *Adv. Funct. Mater.* **30**, 8 (2020).
27. M. Hua et al., Strong tough hydrogels via the synergy of freeze-casting and salting out. *Nature* **590**, 594–599 (2021).
28. T. S. Wheeler, N. D. Sbravati, A. V. Janorkar, Mechanical & cell culture properties of elastin-like polypeptide, collagen, bioglass, and carbon nanosphere composites. *Ann. Biomed. Eng.* **41**, 2042–2055 (2013).
29. B. K. Chan, C. C. Wippich, C.-J. Wu, P. M. Sivasankar, G. Schmidt, Robust and semi-interpenetrating hydrogels from poly(ethylene glycol) and collagen for elastomeric tissue scaffolds. *Macromol. Biosci.* **12**, 1490–1501 (2012).
30. M. Baniasadi, M. Minary-Jolandan, Alginate-collagen fibril composite hydrogel. *Materials (Basel)* **8**, 799–814 (2015).
31. L. Røhl, F. Linde, A. Odgaard, I. Hvid, Simultaneous measurement of stiffness and energy absorptive properties of articular cartilage and subchondral trabecular bone. *Proc. Inst. Mech. Eng. H* **211**, 257–264 (1997).
32. E. Ducrot, Y. Chen, M. Bulters, R. P. Sijbesma, C. Creton, Toughening elastomers with sacrificial bonds and watching them break. *Science* **344**, 186–189 (2014).
33. Y. Xiao, E. A. Friis, S. H. Gehrke, M. S. Detamore, Mechanical testing of hydrogels in cartilage tissue engineering: Beyond the compressive modulus. *Tissue Eng. Part B Rev.* **19**, 403–412 (2013).
34. C. Chen, Z. Wang, Z. Suo, Flaw sensitivity of highly stretchable materials. *Extreme Mech. Lett.* **10**, 50–57 (2017).
35. V. Tutwiler et al., Rupture of blood clots: Mechanics and pathophysiology. *Sci. Adv.* **6**, eabc0496 (2020).
36. R. F. Loeser, Integrin-mediated attachment of articular chondrocytes to extracellular matrix proteins. *Arthritis Rheum.* **36**, 1103–1110 (1993).
37. J. I. Pulai, M. Del Carlo Jr., R. F. Loeser, The α5β1 integrin provides matrix survival signals for normal and osteoarthritic human articular chondrocytes in vitro. *Arthritis Rheum.* **46**, 1528–1535 (2002).
38. K. A. Jansen et al., The role of network architecture in collagen mechanics. *Biophys. J.* **114**, 2665–2678 (2018).
39. M. Castilho et al., Mechanical behavior of a soft hydrogel reinforced with three-dimensional printed microfibre scaffolds. *Sci. Rep.* **8**, 1245 (2018).
40. J. Visser et al., Reinforcement of hydrogels using three-dimensionally printed microfibres. *Nat. Commun.* **6**, 6933 (2015).
41. O. Bas et al., Enhancing structural integrity of hydrogels by using highly organised melt electrospun fibre constructs. *Eur. Polym. J.* **72**, 451–463 (2015).
42. N. Bhardwaj, S. C. Kundu, Electrospinning: A fascinating fiber fabrication technique. *Biotechnol. Adv.* **28**, 325–347 (2010).
43. A. Agrawal, N. Rahbar, P. D. Calvert, Strong fiber-reinforced hydrogel. *Acta Biomater.* **9**, 5313–5318 (2013).
44. S. Lin et al., Design of stiff, tough and stretchy hydrogel composites via nanoscale hybrid crosslinking and macroscale fiber reinforcement. *Soft Matter* **10**, 7519–7527 (2014).
45. W. Sun, J. Paulovich, V. Webster-Wood, Tuning the mechanical and geometric properties of electrochemically aligned collagen threads toward applications in biohybrid robotics. *J. Biomech. Eng.* **143**, 051005 (2021).
46. J. L. Puetzer, T. Ma, I. Sallent, A. Gelmi, M. M. Stevens, Driving hierarchical collagen fiber formation for functional tendon, ligament, and meniscus replacement. *Biomaterials* **269**, 120527 (2021).
47. V. L. Cross et al., Dense type I collagen matrices that support cellular remodeling and microfabrication for studies of tumor angiogenesis and vasculogenesis in vitro. *Biomaterials* **31**, 8596–8607 (2010).
48. K. Ulbrich et al., Targeted drug delivery with polymers and magnetic nanoparticles: Covalent and noncovalent approaches, release control, and clinical studies. *Chem. Rev.* **116**, 5338–5431 (2016).
49. A. Sedlmeier, H. H. Gorris, Surface modification and characterization of photon-upconverting nanoparticles for bioanalytical applications. *Chem. Soc. Rev.* **44**, 1526–1560 (2015).
50. N. Diamantides et al., Correlating rheological properties and printability of collagen bioinks: The effects of riboflavin photocrosslinking and pH. *Biofabrication* **9**, 034102 (2017).
51. C. B. Raub et al., Noninvasive assessment of collagen gel microstructure and mechanics using multiphoton microscopy. *Biophys. J.* **92**, 2212–2222 (2007).
52. Z.-Q. Gu, J.-M. Xiao, X.-H. Zhang, The development of artificial articular cartilage–PVA-hydrogel. *Biomed. Mater. Eng.* **8**, 75–81 (1998).
53. H. Tada, P. C. Paris, G. R. Irwin, *The Stress Analysis of Cracks Handbook, Third Edition* (2000).
54. S. C. Chang et al., Injection molding of chondrocyte/alginate constructs in the shape of facial implants. *J. Biomed. Mater. Res.* **55**, 503–511 (2001).
55. L. R. Bartell, L. A. Fortier, L. J. Bonassar, I. Cohen, Measuring microscale strain fields in articular cartilage during rapid impact reveals thresholds for chondrocyte death and a protective role for the superficial layer. *J. Biomech.* **48**, 3440–3446 (2015).